Soil Dynamics and Earthquake Engineering 199 (2025) 109699

Contents lists available at ScienceDirect

Soil Dynamics and Earthquake Engineering

journal homepage: www.elsevier.com/locate/soildyn

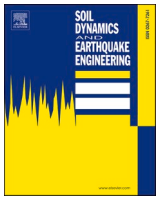

Evaluating the ratio of peak ground acceleration to peak ground velocity from the response spectrum

Longfei You [a], Yan-Gang Zhao [a], Haizhong Zhang [b,*]

[a] Key Laboratory of Urban Security and Disaster Engineering of Ministry of Education, Beijing University of Technology, Beijing, 100124, China
[b] Eco-Science Course, Faculty of Agriculture, Yamagata University, 1-23, Wakaba-machi, Tsuruoka-shi, Yamagata, 997-8555, Japan

ARTICLE INFO

Keywords:
A/V ratio
Displacement response spectrum
Random vibration theory
Centroid frequency of displacement response spectrum

ABSTRACT

The ratio of the peak ground acceleration to the peak ground velocity, referred to as the A/V ratio, is a useful indicator of the frequency content of ground motion and is widely used in earthquake engineering and seismology to estimate structural damage and soil liquefaction potential. The A/V ratio can be calculated using the ground motion prediction equations (GMPEs) based on the information about the source, path, and site. However, in many practical situations, only the response spectrum is available. In this study, a method has been proposed for estimating the A/V ratio from the response spectrum. Firstly, the A/V ratio has been analyzed using the random vibration theory, showing that its square approximately equals the second-order radius of gyration of the Fourier amplitude spectrum and is related to the centroid frequency of the displacement response spectrum. Subsequently, a practical regression formula for the A/V ratio has been developed as a function of the centroid frequency of the displacement response spectrum based on a statistical analysis of 16,000 real seismic records from Japan. Finally, the A/V ratios calculated using the proposed method have been compared with those obtained from the traditional approach based on GMPEs to assess the accuracy of the proposed method.

1. Introduction

The ratio of the peak ground acceleration (PGA) to the peak ground velocity (PGV), referred to as the A/V ratio, is an important and practically useful indicator that reflects the frequency content of seismic ground motion and has been widely used in earthquake engineering and seismology. Tso et al. [1] found significant differences between the frequency content and energy distribution of ground motions with different A/V ratios. Zhu et al. [2] observed that the A/V ratio is closely related to structural damage, with ground motions having lower A/V values tending to cause greater cumulative damage, based on statistical analyses of the inelastic responses of single-degree-of-freedom stiffness-degrading systems. Habib et al. [3] and Castaldo and Tubaldi [4] reached conclusions consistent with those of Zhu et al. [2] through nonlinear time-history analyses of base-isolated structures. In addition, Liao et al. [5] found that the A/V ratio is a critical parameter that governs the response characteristics of medium- and short-period base-isolated bridges by significantly affecting the base shear and displacement demands. Zhang et al. [6] determined the standard response spectrum for near-fault ground motions by utilizing the A/V ratio as a key parameter. Orense [7] found that the A/V ratio is closely related to soil liquefaction potential and proposed a depth reduction factor for assessing liquefaction potential based on the A/V ratio.

The A/V ratio can be calculated using ground motion prediction equations (GMPEs), based on the information about the source, path, and site. Sawada et al. [8] proposed a GMPE for an A/V ratio that considers the effects of the magnitude of the earthquake, its distance, and duration based on a regression analysis of 100 seismic records. Jafarian et al. [9] developed an A/V-ratio GMPE using a genetic programming approach based on the strong ground motion extension database published by the Pacific Earthquake Engineering Research Center.

The A/V ratio can also be calculated using a set of GMPEs for PGA and PGV. Kale et al. [10] proposed GMPEs for PGA and PGV applicable to Turkey and Iran, based on a subset of the compiled strong-motion database from the Middle East Seismic Model Project. Boore et al. [11] proposed GMPEs for PGA, PGV, and response spectra, based on a global database containing events with magnitudes from 3.0 to 7.9, applicable to shallow crustal earthquakes in active tectonic regions. Zhang et al. [12] proposed GMPEs for PGA, PGV, and response spectra applicable to southwest China based on a database with magnitudes ranging from 4.2 to 7.9.

* Corresponding author.
E-mail address: zhang@tds1.tr.yamagata-u.ac.jp (H. Zhang).

https://doi.org/10.1016/j.soildyn.2025.109699
Received 1 May 2025; Received in revised form 23 July 2025; Accepted 23 July 2025

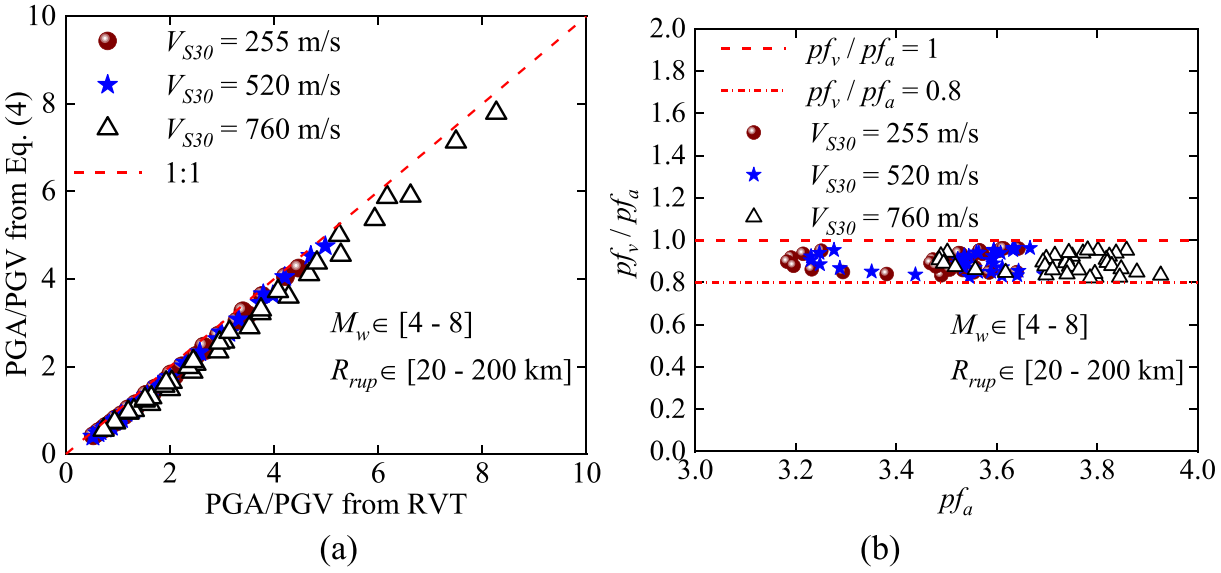

Fig. 1. (a) Comparison of the PGA/PGV results calculated by Eq. (4) and those obtained from RVT. (b) Comparison of the pf_a and pf_v values.

The two aforementioned approaches for estimating the A/V ratio can be used when the A/V-ratio GMPE or both, the GMPEs for PGA and PGV, as well as the required information about the source, path, and site are available. However, in many practical situations, only the response spectrum is available. For example, most worldwide seismic codes [13, 14] specify only the pseudo-acceleration response spectrum as the seismic input for structural design, without GMPEs for PGA and PGV, or for the A/V-ratio, and without any information about the source, path, or site.

Therefore, this paper aims to propose a formula for estimating the A/V ratio from the pseudo-acceleration response spectrum or displacement response spectrum. The remainder of the paper has been organized as follows: Section 2 presents a theoretical analysis of the A/V ratio based on the random vibration theory. Section 3 overviews the strong-motion record database collated from the strong-motion seismograph networks in Japan (K-NET and KiK-net) along with the data processing methods applied in this study. Section 4 presents a practical regression formulation for the A/V ratio based on the statistical analysis of the selected real seismic records. Section 5 presents the results of the comparison between the A/V ratios calculated using the proposed formulation and those obtained from the traditional approach based on GMPEs. Section 6 presents the results of the application of the proposed formulation to calculate the A/V ratios from a design spectrum specified in Minimum Design Loads and Associated Criteria for Buildings and Other Structures (ASCE 7–22 [13]). Finally, Section 7 summarizes the main conclusions of this study.

2. Theoretical analysis of the A/V ratio based on the random vibration theory

To develop a formula for estimating the A/V ratio from spectral displacement (SD) or pseudo-spectral acceleration (PSA), a theoretical analysis of the A/V ratio was conducted based on the random vibration theory (RVT). According to Boore [15], PGA and PGV can be calculated using the following equations:

$$\mathrm{PGA} = pf_a \sqrt{\frac{2}{D_{gm}} \int_0^\infty |Y_a(f)|^2 df} \tag{1}$$

$$\mathrm{PGV} = pf_v \sqrt{\frac{2}{D_{gm}} \int_0^\infty |Y_v(f)|^2 df} \tag{2}$$

where pf_a and pf_v are the peak factors of the ground-motion acceleration and velocity, respectively, D_{gm} is the significant duration used for estimating PGA as well as PGV, f is the frequency, and $Y_a(f)$ and $Y_v(f)$ are the Fourier amplitude spectra (FAS) of the ground-motion acceleration and velocity, respectively. In Eqs. (1) and (2), the ground motion FAS $Y_a(f)$ and $Y_v(f)$ are governed by seismological factors, including the earthquake source, propagation path, and site conditions. Many FAS models have been developed to date [16–18], which are typically expressed as the product of the source term, $E(M_w,f)$, path term, $P(R_{rup}, f)$, and site term, $G(f)$ as follows:

$$Y_a(f) = E(M_w,f)P(R_{rup},f)G(f) \tag{3}$$

where M_w is the moment magnitude and R_{rup} is the rupture distance.

The A/V ratio can be obtained by dividing Eq. (1) by Eq. (2). Although pf_a and pf_v are theoretically different, since pf_a is estimated from the acceleration FAS, whereas pf_v is estimated from the velocity FAS, their results turn out to be very similar (as detailed below). Furthermore, since $Y_a(f) = 2\pi f\, Y_v(f)$, the A/V ratio can be expressed as follows:

$$\mathrm{A} \Big/ \mathrm{V} \approx \sqrt{\frac{\int_0^\infty (2\pi f)^2 |Y_v(f)|^2 df}{\int_0^\infty |Y_v(f)|^2 df}} \tag{4}$$

where $\frac{\int_0^\infty (2\pi f)^2 |Y_v(f)|^2 df}{\int_0^\infty |Y_v(f)|^2 df}$ represents the second-order radius of gyration of the FAS, which characterizes the distribution of energy in the frequency domain.

To check the accuracy of the derived equation (Eq. (4)), a point-source FAS model proposed by Boore [15] was applied to calculate the A/V ratio. The seismic parameters used in the FAS model were consistent with those of Zhang et al. [19]. A wide range of moment magnitudes (M_w = 4–8), rupture distance (R_{rup} = 20–200 km), and time-averaged shear-wave velocities of the upper 30 m (V_{S30} = 255 m/s [20], V_{S30} = 520 m/s [20], and V_{S30} = 760 m/s [21]) were used for the calculations. The A/V ratios calculated from Eq. (4) were compared with those from RVT obtained using Eqs. (1) and (2) and the results are shown in Fig. 1(a). The good agreement between the ratios obtained by both methods confirms the accuracy of Eq. (4). In addition, values of pf_a and pf_v are compared in Fig. 1(b). The similarity between the values of pf_a and pf_v for the two methods further supports the rationality of the derivation of Eq. (4).

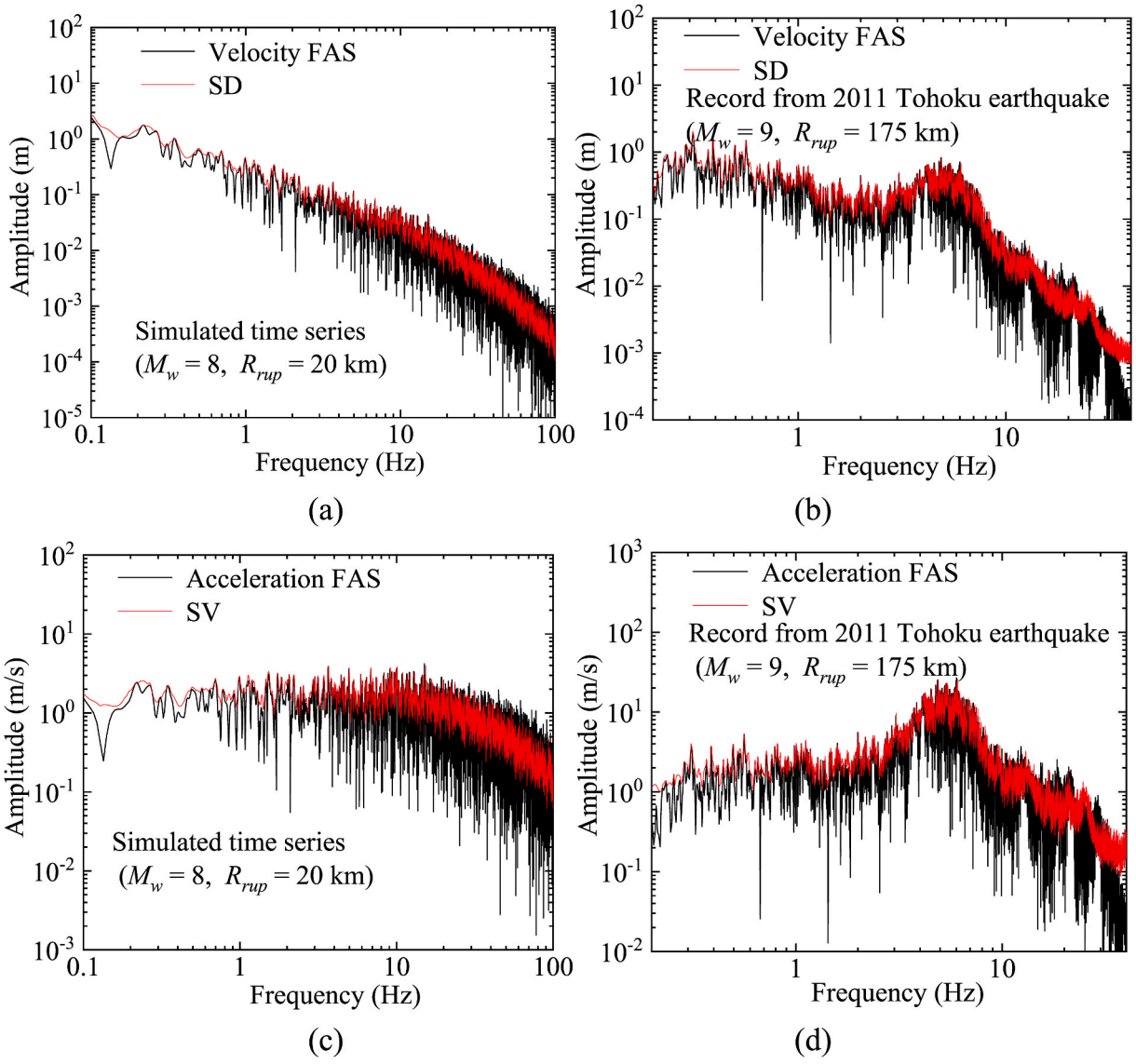

Fig. 2. Comparison of the acceleration FAS and SV using a (a) simulated time series and (b) real seismic record. Comparison of the velocity FAS and SD using a (c) simulated time series and (d) real seismic record.

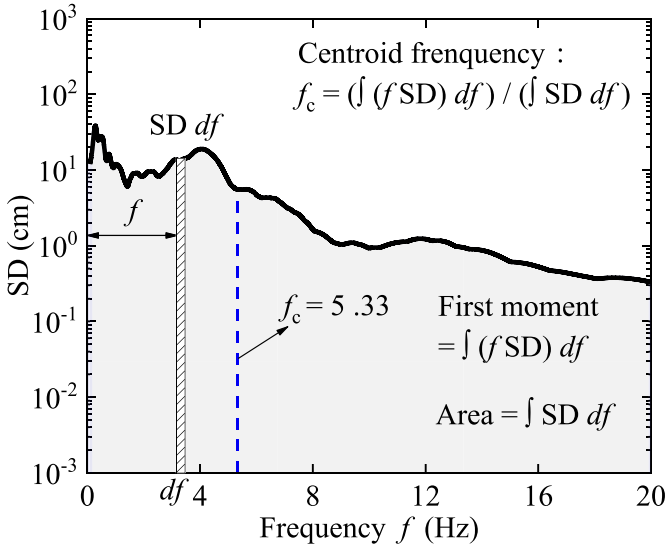

Fig. 3. Illustration of the physical meaning of the centroid frequency, f_c, of the SD.

Equation (4) establishes the relationship between the A/V ratio and the velocity FAS. However, the objective of this study is to determine the A/V ratio from the response spectra (SD or PSA). Thus, it is necessary to replace the velocity FAS in Eq. (4) with SD or PSA. It has been reported that the acceleration FAS is similar to the undamped spectral velocity (SV) [22]. Moreover, the relationship between the acceleration FAS and the velocity FAS satisfies $Y_a(f) = 2\pi f\, Y_v(f)$, and the relationship between SV and SD satisfies $SV \approx 2\pi f\, SD$. Therefore, it can be inferred that the velocity FAS is similar to the undamped SD.

In order to check the rationality of the above inference, the velocity FAS and undamped SD were compared using numerous real earthquake records (detailed in Section 4) and simulated time-series signals. The time-series signals for the analysis were generated from the above FAS using the Stochastic Method SIMulation program [23] through stochastic simulations [24]. The average FAS of the simulated time series matched the target FAS derived from the point-source model, whereas the phase of each time series behaved randomly. The representative comparisons of a real earthquake record and a simulated time-series signal are shown in Fig. 2. The M_w of the real earthquake record is 9 and the R_{rup} is 175 km. The M_w of the simulated time-series signal is 8 and the R_{rup} is 20 km. Fig. 2(a) and (b) present a comparison of the results of the velocity FAS and the undamped SD. The consistency between the two verifies the correctness of the above inference. Further, Fig. 2(c) and (d) show the comparison of the results of the acceleration FAS and the undamped SV, and the consistency between them further validates the correctness of the above inference. In addition, the amplitude of SD varies with the damping ratio. However, since SD appears in the numerator as well as the denominator in Eq. (5), the variation in the amplitude of SD is mostly canceled out.

Based on the above inference, the velocity FAS, $Y_v(f)$, in Eq. (4) can be replaced by SD, resulting in

$$\mathrm{A}\Big/\mathrm{V} \approx \sqrt{\frac{\int_0^\infty (2\pi f)^2 SD^2 df}{\int_0^\infty SD^2 df}} \tag{5}$$

Since the 5 % damped response spectrum is commonly used in practice, the damping ratio of SD in Eq. (5) and the following discussions were considered to be 5 %. It is observed that Eq. (5) is relatively

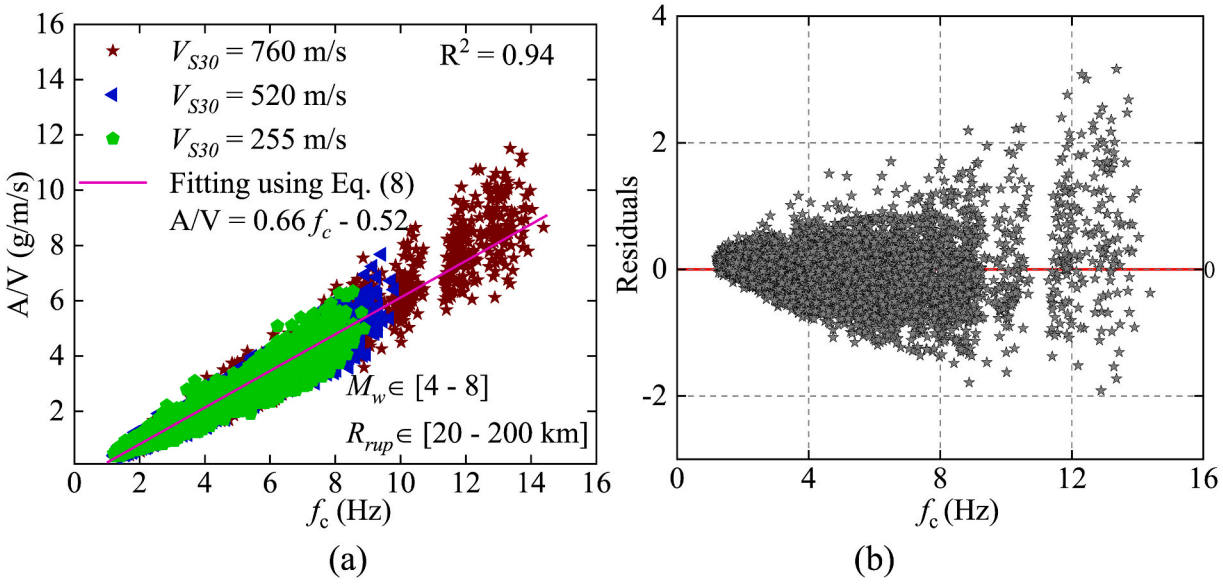

Fig. 4. (a) Regression results of A/V ratio, obtained using Eq. (8), and (b) variation of the residuals of the A/V ratio, as a function of f_c.

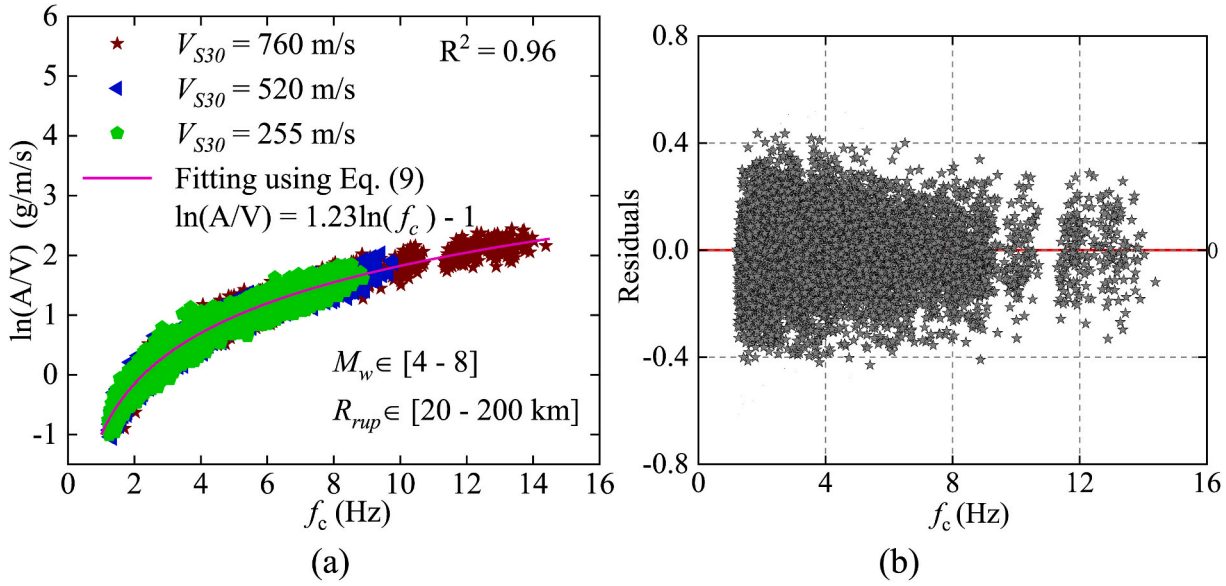

Fig. 5. (a) Regression results of ln(A /V), obtained using Eq. (9), and (b) variation of the residuals of the ln(A/V), as a function of f_c.

complex, prompting further approximation:

$$\mathrm{A}\Big/\mathrm{V}\approx\sqrt{\frac{\int_0^\infty (2\pi f)^2 SD^2 df}{\int_0^\infty SD^2 df}}\approx k\left(\frac{\int_0^\infty fSD\,df}{\int_0^\infty SD\,df}\right)+b \tag{6}$$

where k and b are suitable coefficients. In Eq. (6),

$$f_c=\frac{\int_0^\infty f\,SDdf}{\int_0^\infty SDdf} \tag{7}$$

represents the centroid frequency, f_c, of the SD.

Fig. 3 illustrates the physical meaning of Eq. (7), where $\int_0^\infty f\,SDdf$ represents the first moment of the area formed by the SD and the frequency axis relative to the longitudinal axis, and $\int_0^\infty SDdf$ represents the area formed by the SD and the frequency axis. Therefore, the ratio of $\int_0^\infty f\,SDdf$ and $\int_0^\infty SDdf$ represents the centroid frequency of the SD. It can be noted from Eq. (7) that if SD is available, f_c can be easily computed.

In summary, the relationship between the A/V ratio and f_c can be approximated as follows:

$$\mathrm{A}/\mathrm{V}\approx k f_c+b \tag{8}$$

Thus, the A/V ratio can be related to SD through its centroid frequency, f_c, using Eq. (8). It should be noted that Eq. (8) is not a strict formulation for estimating the A/V ratio from f_c. Instead, it is derived as a functional form expressing the relationship between the A/V ratio and f_c, which will serve as the basis for constructing a formula for estimating the A/V ratio from f_c.

In addition, it should be noted that f_c is derived from the SD related to FAS, which is governed by seismological factors, including the source of the earthquake, its propagation path, and the site conditions. Therefore, f_c reflects the effects of these seismological factors.

To verify the rationality of Eq. (8), the results of the A/V ratio and f_c for the abovementioned simulated time-series signals were calculated and the results have been shown in Fig. 4. It can be seen that the relationship between the A/V ratio and f_c typically satisfies the linear relationship expressed by Eq. (8). When fitting this relationship using Eq. (8), a coefficient of determination (R^2) of 0.94 can be obtained. Nevertheless, Fig. 4(a) shows that the variance of the A/V ratio increases as f_c increases. In addition, Fig. 4(b) shows the variation of the residuals of the A/V ratio as a function of f_c using Eq. (8), indicating a clear presence of heteroscedasticity. Therefore, to mitigate the heteroscedasticity, the logarithm of both sides of Eq. (8) was taken, thereby deriving the following equation:

$$\ln(\mathrm{A}/\mathrm{V})\approx K\ln(f_c)+B \tag{9}$$

where K and B are suitable coefficients.

Fig. 5(a) shows the results obtained by fitting the logarithmic model expressed by Eq. (9), which yielded a coefficient of determination R^2 of 0.96. In addition, the variance of ln(A /V) can be observed to be consistent with increase in f_c. Fig. 5(b) shows the variation of the residuals of ln(A /V), obtained using Eq. (9), as a function of f_c, where the discrete degree of ln(A /V) does not increase as f_c increases, and no obvious heteroscedasticity is observed. Therefore, the functional form expressed by Eq. (9) was considered more reasonable than that expressed by Eq. (8) and was applied to develop the formulation for estimating the A/V ratio from f_c based on real seismic records in Section 4.

Additionally, as shown in Fig. 4(a) and 5(a), ln(A /V) and f_c exhibit different ranges of variation across different site classes. The variation range of the A/V ratio and f_c become narrower and the variation in their upper limits decreases as V_{S30} decreases. Nevertheless, the functional form of Eq. (9) remains valid in capturing the relationship between the A/V ratio and f_c across different site conditions.

3. Strong-motion database and data processing method

3.1. Strong-motion database

To establish a model for estimating the A/V ratio from the SD, 16,000 real seismic records were collected from strong-motion seismograph networks K-NET and KiK-net [25–27]. The K-NET and KiK-net networks provide only the magnitudes, M_j, and epicentral distances, R_e, from the Japan Meteorological Agency. However, the moment magnitude, M_w, and rupture distance, R_{rup}, are more commonly used. For most of the selected records, the M_w and R_{rup} can be obtained from the flatfile compiled by Morikawa et al. [28]. For records not included in this flatfile, M_j was converted to M_w using the formula given by Uchide and Imanishi [29], and R_{rup} was calculated using finite-fault models or simplified geometric methods. The M_w values for these selected records ranged from 3.7 to 9 and the R_{rup} values ranged from 10 to 250 km.

The selected ground motions were recorded at 338 stations, which were divided into four site classes (B, C, D, and E) based on the V_{S30}, as

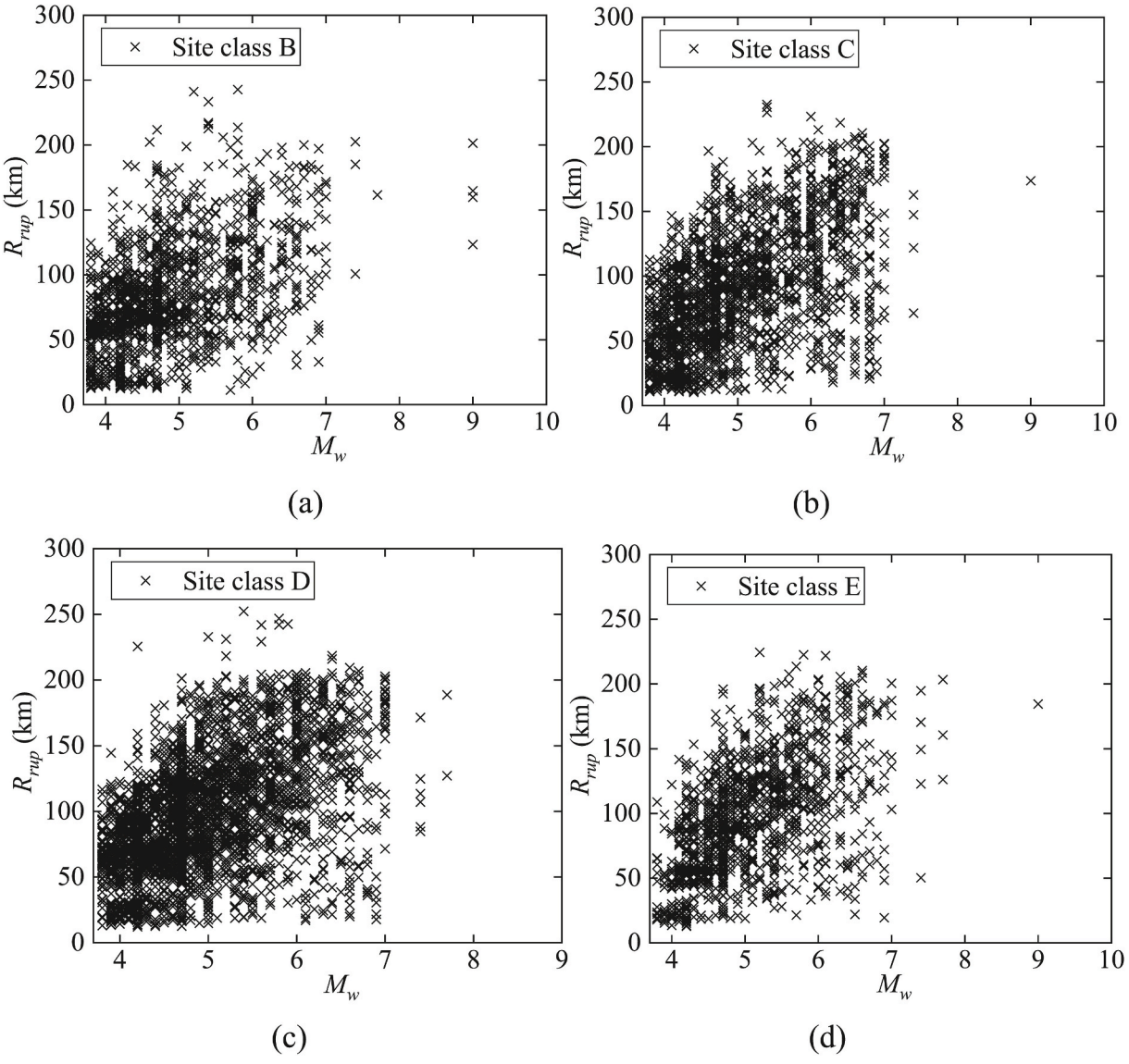

Fig. 6. Distribution of M_w and R_{rup} of ground motions recorded at site class (a) B, (b) C, (c) D, and (d) E.

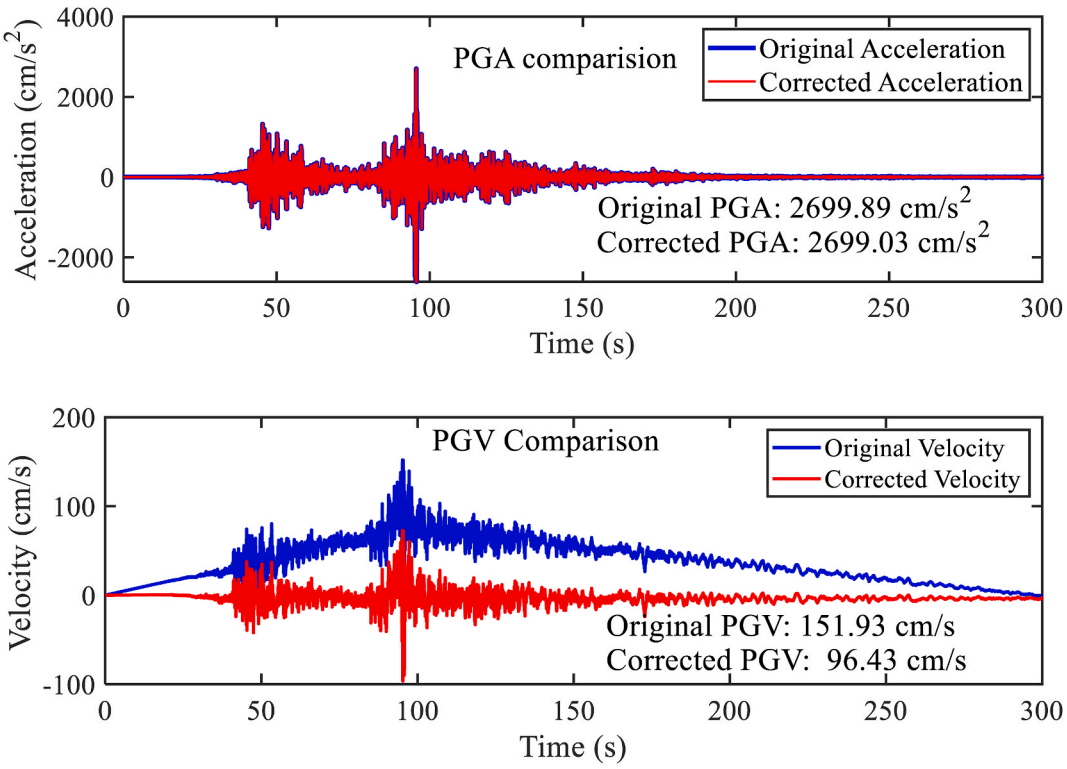

Fig. 7. Example of baseline correction done using the algorithm of Sigurdsson et al. [30].

specified by the National Earthquake Hazards Reduction Program [30]. This study excluded site class A because there were few sites belonging to this class in the K-NET and KiK-net databases. The distributions of M_w and R_{rup} for the four site classes are shown in Fig. 6.

3.2. Data processing method

When calculating the A/V ratio from a real seismic record, PGA as well as PGV needs to be determined. Since PGA is less affected by noise, it can be easily obtained from the acceleration time series. However, obtaining a reliable PGV requires careful processing of seismic records. This is because when integrating the acceleration time series to obtain the velocity time series, noise may introduce a baseline offset in the velocity time series, leading to significant errors in the calculated PGV [31]. To address this issue, the baseline correction algorithm proposed by Sigurdsson et al. [32] was used to remove noise from the seismic records. This baseline correction algorithm applies an automated iterative baseline correction to the acceleration time series based on the seismic source spectra theory, with the flatness of the displacement FAS in the low-frequency range serving as an objective constraining criterion.

Fig. 7 presents an example of the baseline correction applied to a real earthquake record. Due to noise, the calculated velocity waveform initially exhibited a bilinear baseline drift. However, after baseline correction, the velocity waveform stabilized. In addition, it can be seen from the figure that the baseline correction applied to the velocity time series does not affect the acceleration time series. The PGV before the correction was 57 % higher than the corrected value, whereas PGA showed negligible changes before and after the correction.

4. Practical regression formula for the A/V ratio based on statistical analysis

To obtain a formula for the A/V ratio based on the SD using Eq. (9), a statistical analysis was conducted using the real seismic records described in Section 3. The results of the regression analysis, including the values of the coefficients K and B, are shown in Fig. 8. To examine the impact of site effects, the sites were categorized into four classes (B, C, D, and E) based on V_{S30} and a separate regression analysis was performed for each class.

As illustrated in Fig. 8, $\ln(A/V)$ consistently increases with f_c across all site classes. The coefficient of determination for the $\ln(A/V)$ and f_c relationships across all site classes is approximately 0.9, and the standard deviation of residuals for the four site groups remains consistently around 0.15. Furthermore, majority of the actual data points fall within the 95 % confidence intervals of the fitting results. Fig. 9 shows the variation of the residuals of $\ln(A/V)$ as a function of f_c for the four site classes, where the degree of dispersion in $\ln(A/V)$ remains nearly constant as f_c increases, and no obvious heteroscedasticity is observed. In conclusion, the fitting results for all four site classes demonstrate a high degree of reliability.

In addition, the results of $\ln(A/V)$ and f_c calculated from the simulated time series in Section 2 are also plotted in Fig. 8. As observed from Fig. 8, although Eq. (9) is derived using real seismic records, its results align well with those from the simulated time series, further validating the proposed formulation. In addition, the results from the simulated time series are in good agreement with the real seismic records, verifying the rationality of the theoretical derivation in Section 2.

As shown in Fig. 8, $\ln(A/V)$ and f_c exhibit different ranges of variation across different site classes. The variation range of $\ln(A/V)$ and f_c becomes narrower as the site changes from hard to soft. The variation range of the A/V ratio for sites B, C, D, and E are 0.6–20 g/m/s, 0.4–14 g/m/s, 0.4–10 g/m/s, and 0.4–7 g/m/s, respectively. The variation range of f_c for site classes B, C, D, and E are 1–18 Hz, 1–16 Hz, 1–13Hz, and 1–11Hz, respectively. It can be noted that as the site changes from hard to soft, the upper limits of the variations in both $\ln(A/V)$ and f_c decrease. This variation pattern of $\ln(A/V)$ and f_c with site conditions is consistent with that obtained from the simulated time series in Section 2 (Fig. 5(a)).

The different variation ranges of $\ln(A/V)$ and f_c across different site

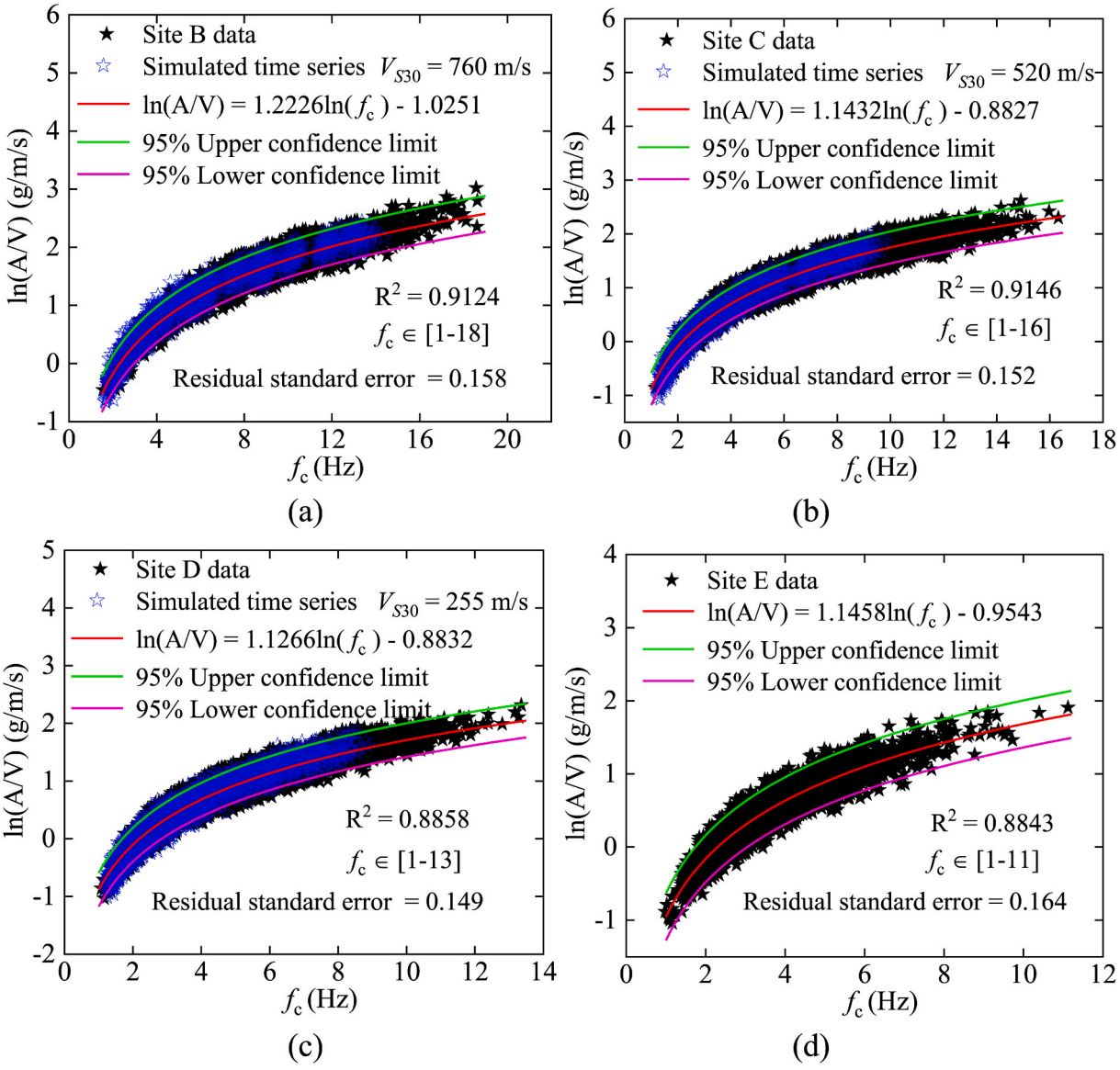

Fig. 8. Regression relationship between ln(A/V), obtained using Eq. (9), and f_c, for site class (a) B, (b) C, (c) D, and (d) E.

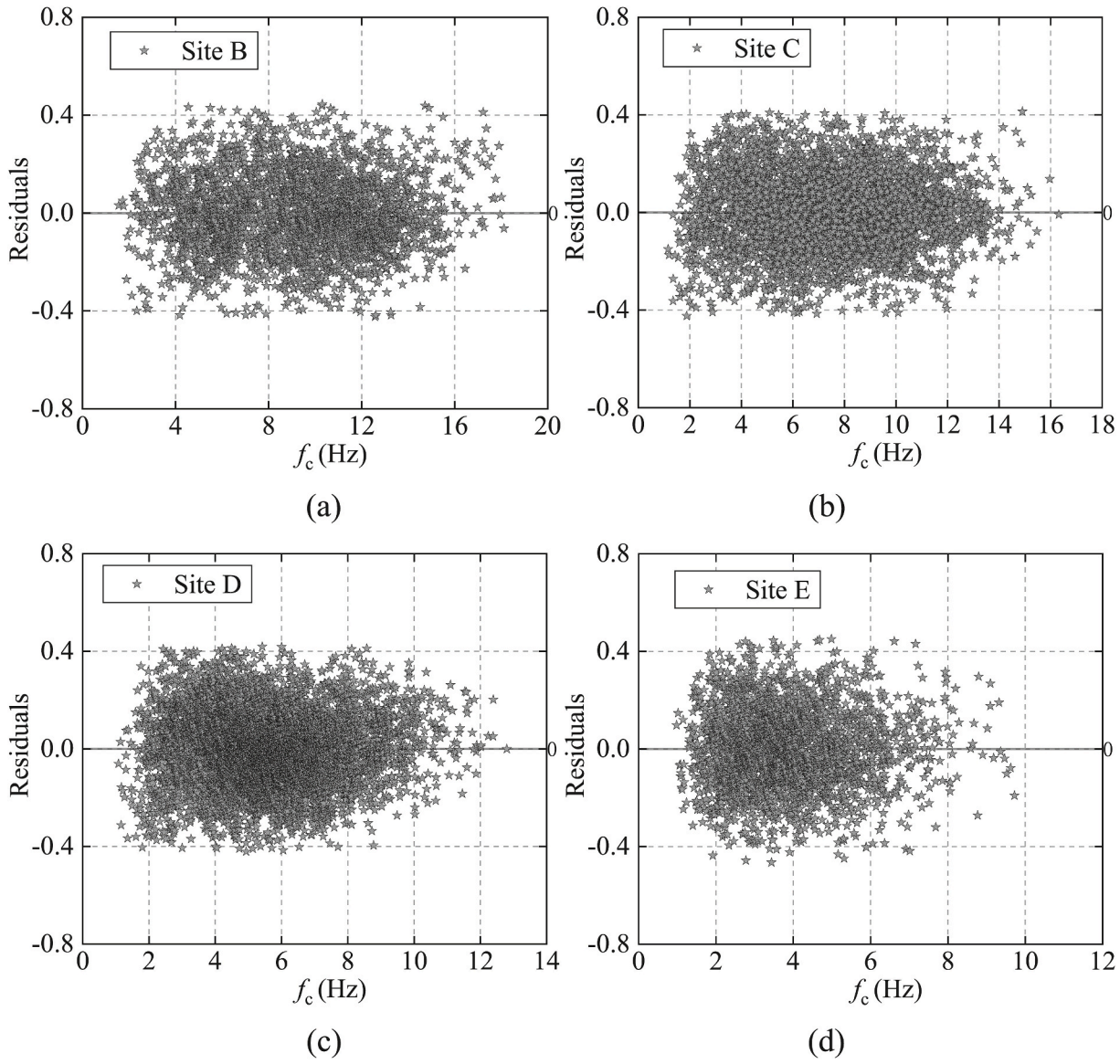

Fig. 9. Variation of the residuals of ln(A/V), obtained using Eq. (9), as a function of f_c for site class (a) B; (b) C, (c) D, and (d) E.

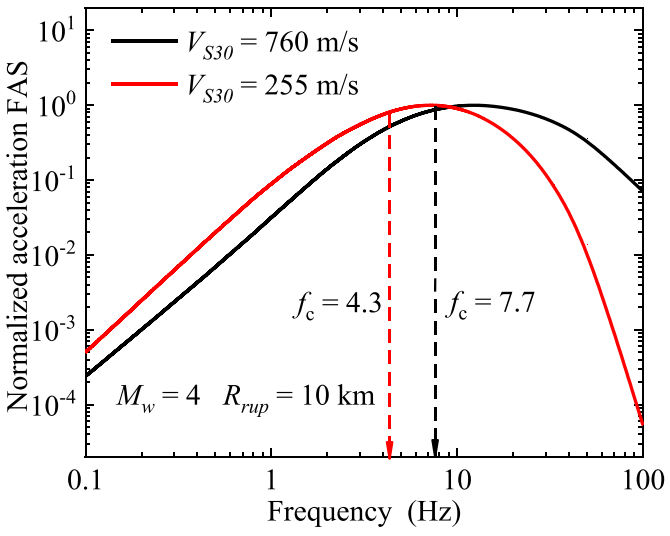

Fig. 10. Comparison of acceleration FAS for different site conditions.

classes are primarily attributed to site effects on the frequency content of ground motion. Local site conditions act as a filter that alters the frequency content of ground motion. For harder sites, the fundamental frequency of the site is larger, which amplifies the high-frequency components more significantly. In contrast, for softer sites, the fundamental frequency is smaller, which amplifies the lower-frequency components significantly. This results in a larger f_c for harder sites and a smaller f_c for softer sites. Fig. 10 shows a comparison of the acceleration FAS for the harder and softer sites. As observed from Fig. 10, as the site becomes harder, the high-frequency components of the acceleration FAS increase, leading to an increase in f_c.

Regression analysis was also conducted for all the seismic records in the four site classes, as shown on Fig. 11. Although site conditions influence the variation range of the A/V ratio and f_c, they do not affect the relationship between them. As shown in Fig. 11, the trend of the variation between the A/V ratio and f_c remains consistent across different site classes (B, C, D, or E). Fig. 12 compares the regression models for estimating the A/V ratio from f_c based on seismic records from different site classes. It can be observed that the regression models are largely consistent, even the seismic records used for regression are from different site classes. This suggests that incorporating site conditions

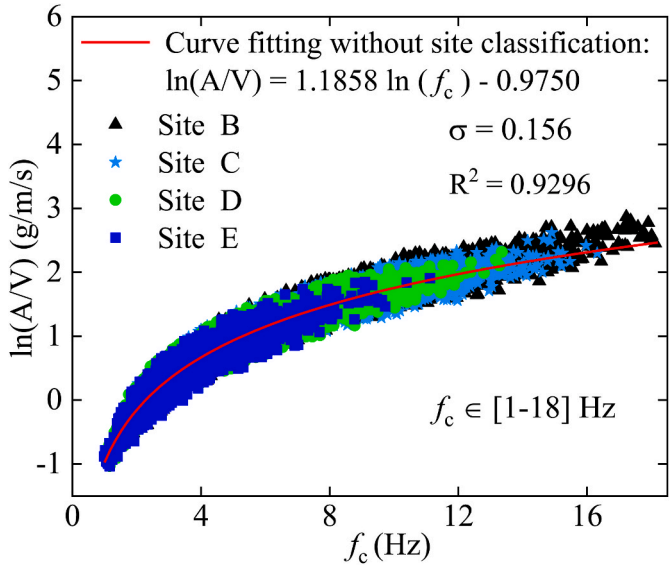

Fig. 11. Regression relationship between ln(A/V), obtained using Eq. (9), and f_c based on all seismic records across different site classes.

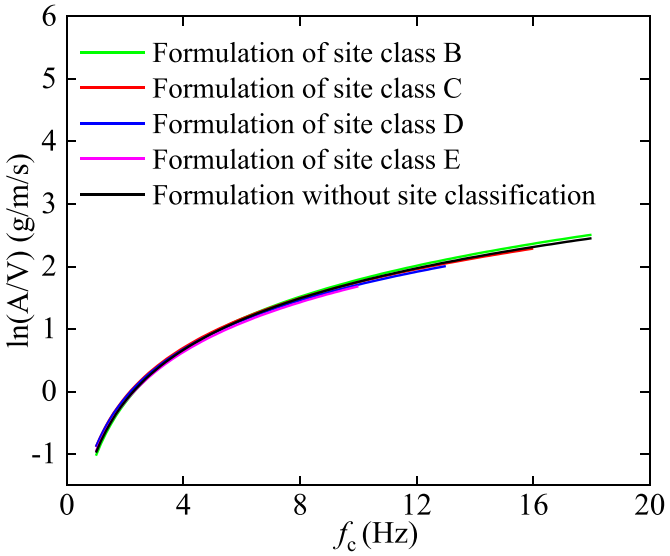

Fig. 12. Comparison of the regression models based on seismic records from different site classes.

into the model for estimating the A/V ratio from f_c is unnecessary. Therefore, the regression model shown in Fig. 11 was adopted as the proposed formulation, which can be expressed as follows:

$$\ln(A/V) = 1.1858 \ln(f_c) - 0.9750 \quad (10)$$

Here, the standard deviation, σ, of the proposed formulation is 0.156.

Eq. (10) is applicable for estimating the A/V ratio from f_c for any site conditions. In addition, since the range of f_c for the seismic records used in the regression is between 1 and 18 Hz, the applicable range of Eq. (10) is also limited to this range.

5. Comparison of the proposed formulation with the traditional approach using GMPEs

This section presents a comparison of the A/V ratios calculated using the proposed formulation with those obtained from the traditional approach based on GMPEs. The GMPE models proposed by Boore et al. [11] and Zhang et al. [12] were chosen for the comparison as they provide GMPEs for PGA, PGV, and also 5 %-damped PSA, allowing the calculation of the A/V ratios as well as f_c values. The GMPEs proposed by Boore et al. [11] were developed based on the earthquake data from California, Taiwan, and New Zealand. The GMPEs proposed by Zhang et al. [12] were developed based on the earthquake data from Western China. A wide range of magnitudes, distances, and site conditions were considered to calculate the values of A/V ratios and f_c.

Figs. 13 and 14 show a comparison of the results obtained from the GMPEs proposed by Boore et al. [11] and Zhang et al. [12], real seismic records from Japan, and the formulation proposed in this study. As shown in the figure, the results obtained from the GMPEs proposed by Boore et al. [11] and Zhang et al. [12] align well with those from the real records and the proposed formulation across site classes B, C, D, and E, thereby demonstrating the accuracy of the proposed formulation. Moreover, despite these GMPEs being derived from earthquake data from California, Taiwan, New Zealand, and western China, and the proposed formulation being based on the earthquake records only from Japan, the results were very similar, suggesting that the proposed formulation is applicable to different regions.

6. Application of the proposed formulation

The formulation proposed in this study was applied to calculate the A/V ratios from the design spectra in ASCE 7–22 [13]. Four sites in the United States, with longitudes and latitudes (33.4484°N, 112.0740°W), (40.7128°N, 74.0060°W), (42.3601°N, 71.0589°W), and (36.1699°N, 115.1398°W), were randomly selected for the calculations. The design spectra were constructed based on the short period and 1-s period, and the long-period transition period spectral accelerations. These spectral accelerations were determined for the 0.2 % annual exceedance probability from the seismic hazard map. In addition, 100 real seismic records were selected from the Pacific Earthquake Engineering Research Center database that matched the design spectra. As shown in Fig. 15, the average values of the spectra for the 100 real seismic records closely aligned with the design spectra values. The seismic records selected for this study covered multiple seismically active regions worldwide, including the western United States, Taiwan region, Europe region, and western China, in order to validate the broad range of applicability of the proposed A/V ratio formulation. The A/V ratio and f_c of each seismic record and the average values of 100 seismic records were calculated

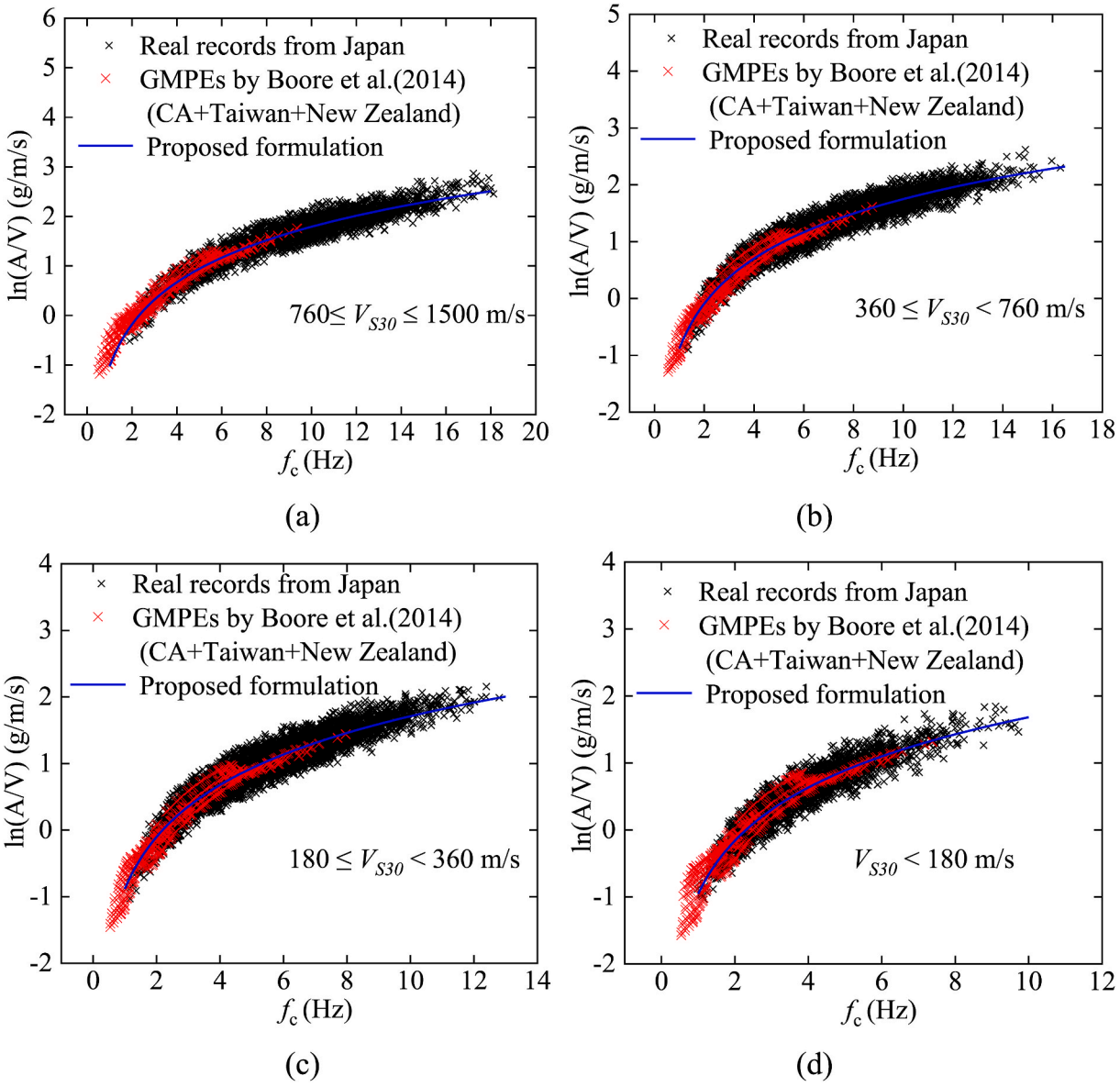

Fig. 13. Comparison of the A/V ratios from the GMPE model by Boore et al. [11], real records from Japan, and the proposed formulation for site class (a) B, (b) C, (c) D, and (d) E.

and compared with those obtained using the proposed formulation, as shown in Fig. 16.

It can be seen from the figure that the A/V ratios calculated from the 100 seismic records agree well with those obtained by the proposed formulation. Additionally, the calculated results almost all fall within the 95 % confidence interval of the proposed model. Furthermore, the A/V ratio calculated from the design spectra using the proposed formulation is in close agreement with the average A/V ratio of the 100 actual seismic records. These results confirm the accuracy as well as the wide range of applicability of the proposed A/V ratio formulation.

7. Conclusions

In this study, a model was proposed for calculating the ratio of the peak ground acceleration to the peak ground velocity (the A/V ratio) from the response spectrum. First, the A/V ratio was theoretically analyzed based on RVT, revealing its relationship with the centroid frequency of the displacement response spectrum. Then, a practical formulation for the A/V ratio was derived based on the statistical analysis of 16,000 real seismic records from Japan. The main conclusions drawn from this study can be summarized as follows:

1. Analysis based on RVT revealed that the square of the A/V ratio is equal to the second-order radius of gyration of the power spectrum, which characterizes the concentration of energy in the frequency domain.
2. The theoretical relationship between the A/V ratio and centroid frequency derived based on RVT was verified using simulated time-series signals, with a coefficient of determination of 0.96.
3. The proposed A/V ratio formulation obtained from real seismic records exhibited good accuracy across different site classes. The regression results of the A/V ratio for different sites were consistent with each other and the formulation based on all seismic records (ignoring site classification) was applicable to predicting the A/V ratio from the displacement response spectra.
4. The results obtained using the proposed formulation were compared to those obtained using two traditional methods based on GMPEs

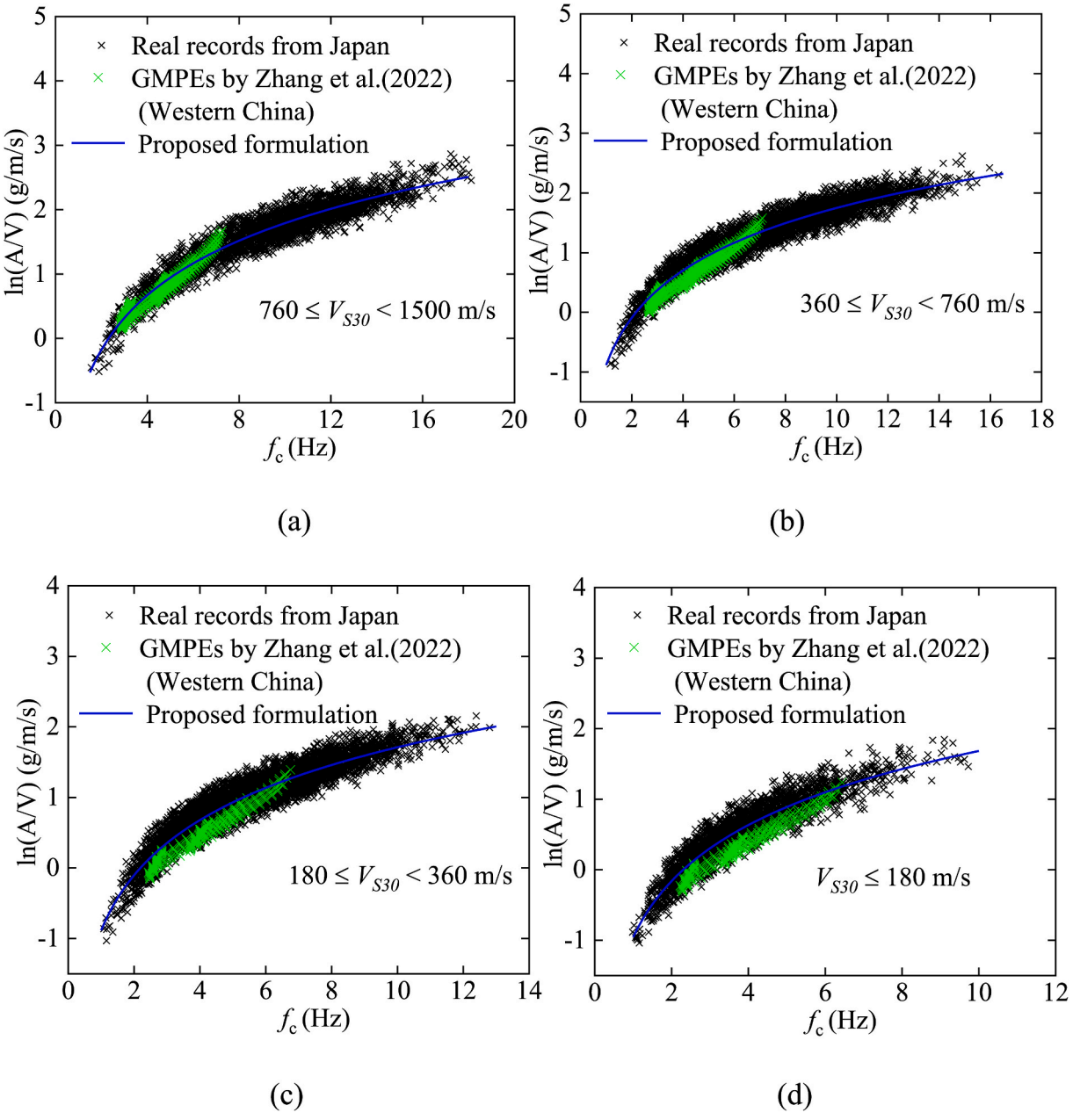

Fig. 14. Comparison of the A/V ratios from the GMPE model by Zhang et al. [12], real records from Japan, and the proposed formulation for site class (a) B, (b) C, (c) D, and (d) E.

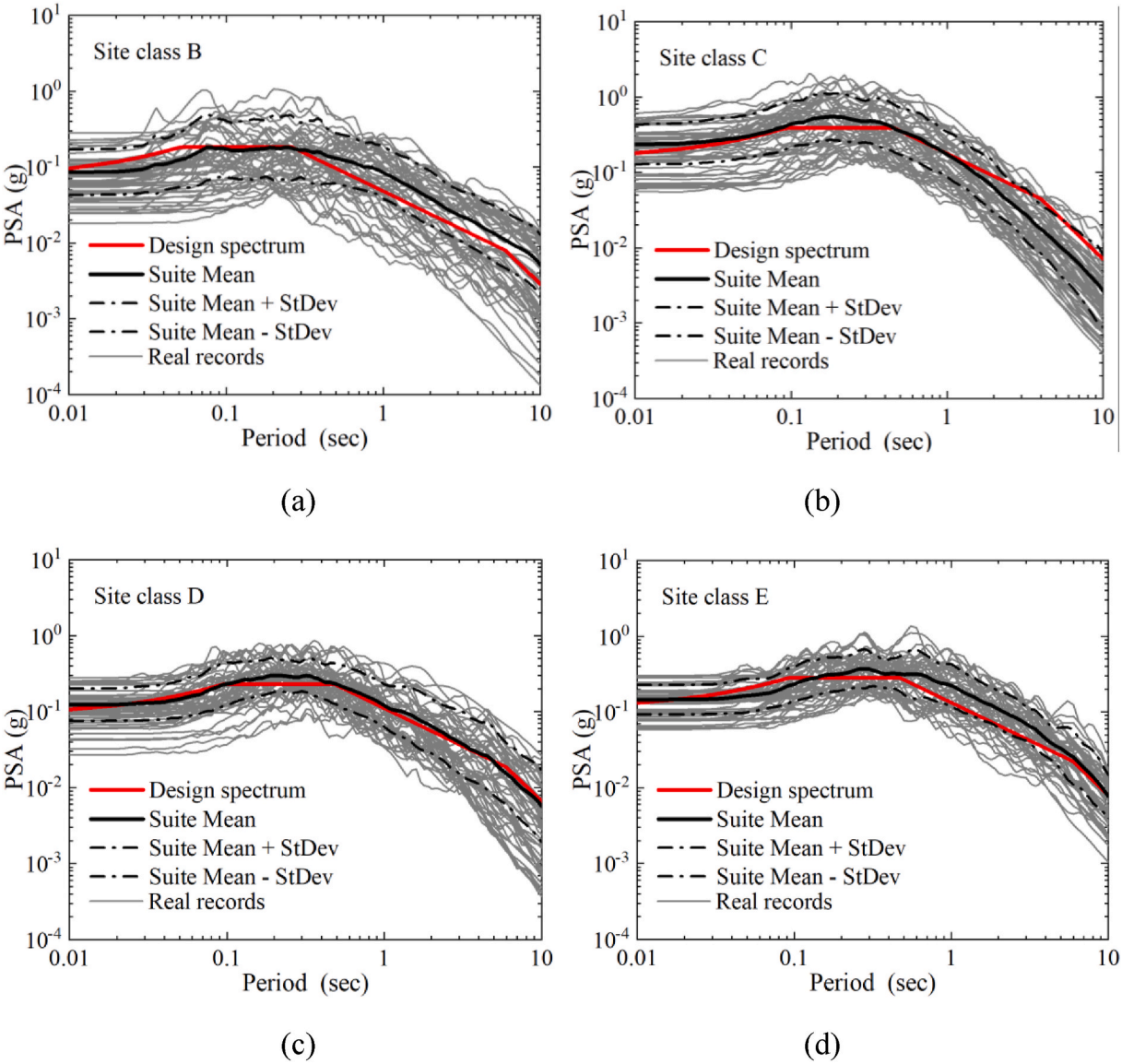

Fig. 15. Comparison of the ASCE 7–22 design spectra and the selected 100 real seismic records for (a) region 1, site class B; (b) region 2, site class C; (c) region 3, site class D; and (d) region 4, site class E.

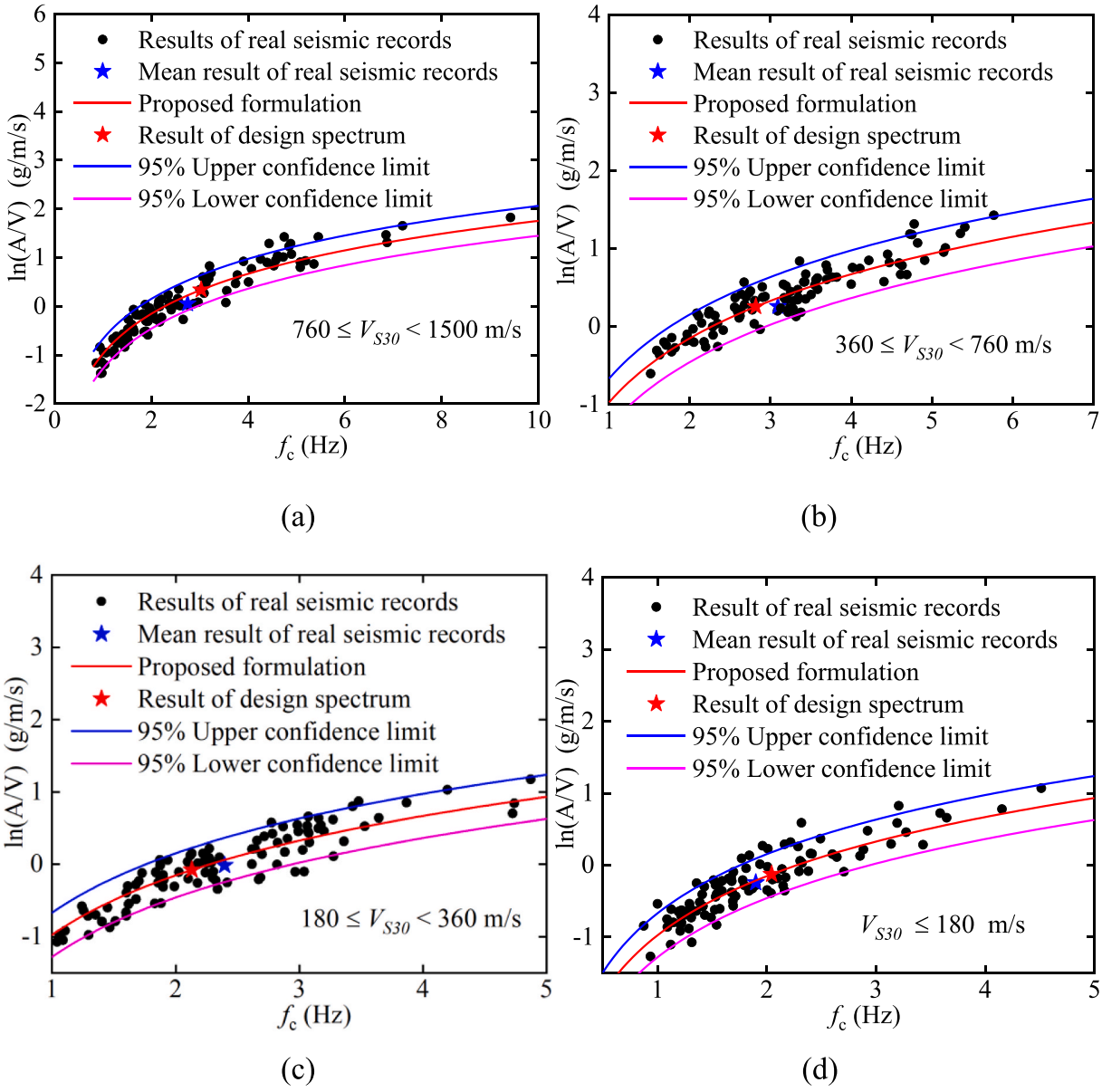

Fig. 16. Comparison of the results obtained using the proposed formulation and those of the actual earthquake records for (a) region 1, site class B; (b) region 2, site class C; (c) region 3, site class D; and (d) region 4, site class E.

(Boore et al., 2014, Zhang et al., 2022) and were found to be consistent.

5. The proposed formulation was applied to calculate the A/V ratio from the design spectra, demonstrating the practical applicability of the formulation.

CRediT authorship contribution statement

Longfei You: Writing – original draft, Visualization, Methodology, Data curation, Conceptualization. **Yan-Gang Zhao:** Writing – review & editing, Supervision, Data curation. **Haizhong Zhang:** Writing – review & editing, Supervision, Methodology, Investigation, Conceptualization.

Code availability

Available upon request.

Statement of originality

Existing studies mostly rely on ground motion prediction equations (GMPEs) or statistical methods to estimate A/V ratios, but lack theoretical support in scenarios with only response spectra. Based on the random vibration theory, this study reveals for the first time that the square of the A/V ratio is equal to the second-order radius of gyration of the Fourier amplitude spectrum, and derives its explicit relationship with the centroid frequency of the displacement response spectrum. The accuracy of the proposed regression formula (coefficient of determination >0.88) is verified by statistical analysis of 16,000 measured seismic records in Japan, which proves that it is suitable for different site types and regions. The comparison results with the traditional GMPE method are consistent, and the engineering practicability of the method is proved by the application of ASCE 7 design spectrum. The study fills the theoretical gap in the direct estimation of A/V ratio by response spectrum, and provides a new way for the evaluation of ground motion parameters.

Funding

This work was supported by the National Natural Science Foundation of China (Grant No. 52278135) and the National Key R&D Program of China (2023YFC3805100, 2023YFC3805101).

Declaration of competing interest

The authors declare that they have no known competing financial interests or personal relationships that could have appeared to influence the work reported in this paper.

Acknowledgments

We acknowledge the support received from the National Natural Science Foundation of China (Grant No. 52278135) as well as the National Key R&D Program of China (2023YFC3805100, 2023YFC3805101). I would like to sincerely thank the Associate Editor and the reviewers for their valuable time, constructive comments, and insightful suggestions, which have greatly improved the quality of this manuscript.

Data availability

Data will be made available on request.

References

[1] Tso WK, Zhu TJ, Heidebrecht AC. Engineering implication of ground motion A/V ratio. Soil Dynam Earthq Eng 1992;11(3):133–44.
[2] Zhu TJ, Tso WK, Heidebrecht AC. Effect of peak ground a/v ratio on structural damage. J Struct Eng 1988;114(5):1019–37.
[3] Habib A, Houri AAL, Yildirim U. Comparative study of base-isolated irregular RC structures subjected to pulse-like ground motions with low and high PGA/PGV ratios. Structures 2021;31:1053–71.
[4] Castaldo P, Tubaldi E. Influence of ground motion characteristics on the optimal single concave sliding bearing properties for base-isolated structures. Soil Dynam Earthq Eng 2018;104:346–64.
[5] Liao WI, Loh CH, Lee BH. Comparison of dynamic response of isolated and non-isolated continuous girder bridges subjected to near-fault ground motions. Eng Struct 2004;26(14):2173–83.
[6] Zhang C, Wu C, Wang P, Li D, Lu J. Improved methods for synthesizing near-fault ground motions based on specific response spectrum. Soil Dynam Earthq Eng 2024;183:108790.
[7] Orense RP. Assessment of liquefaction potential based on peak ground motion parameters. Soil Dynam Earthq Eng 2005;25(3):225–40.
[8] Sawada T, Hirao K, Yamamoto H, Tsujihara O. Relation between maximum amplitude ratio (a/v, ad/v^2) and spectral parameters of earthquake ground motion. Earthquake engineering. Tenth World Conf 1992;2:617.
[9] Jafarian Y, Kermani E, Baziar MH. Empirical predictive model for the v_{max}/a_{max} ratio of strong ground motions using genetic programming. Comput Geosci 2010;36(12):1523–31.
[10] Kale Ö, Akkar S, Ansari A, Hamzehloo H. A ground-motion predictive model for Iran and Turkey for horizontal PGA, PGV, and 5% damped response spectrum: investigation of possible regional effects. Bull Seismol Soc Am 2015;105(2A):963–80.
[11] Boore DM, Stewart JP, Seyhan E, Atkinson GM. NGA-West2 equations for predicting PGA, PGV, and 5% damped PSA for shallow crustal earthquakes. Earthq Spectra 2014;30(3):1057–85.
[12] Zhang B, Yu Y, Li X, Wang Y. Ground motion prediction equation for the average horizontal component of PGA, PGV, and 5% damped acceleration response spectra at periods ranging from 0.033 to 8.0 s in southwest China. Soil Dynam Earthq Eng 2022;159:107297.
[13] American Society of Civil Engineers. Minimum design loads and associated criteria for buildings and other structures. Am Soc Civi Eng 2022.
[14] Code P. Eurocode 8: design of structures for earthquake resistance-part 1: general rules, seismic actions and rules for buildings. Brussels: European Committee for Standardization; 2005.
[15] Boore DM. Simulation of ground motion using the stochastic method. Pure Appl Geophys 2003;160(3):635–76. https://doi.org/10.1007/PL00012553.
[16] Brune JN. Tectonic stress and the spectra of seismic shear waves from earthquakes. J Geophys Res 1970;75(26):4997–5009.
[17] Atkinson Gail M, Silva Walter. Stochastic modeling of California ground motions. Bull Seismol Soc Am 2000;90(2):255–74. https://doi.org/10.1785/0119990064.
[18] Beresnev IA, Atkinson GM. Modeling finite-fault radiation from the ω^n spectrum. Bull Seismol Soc Am 1997;87(1):67–84.
[19] Zhang H, Zhang R, Zhao YG. Novel approach for energy-spectrum-based probabilistic seismic hazard analysis in regions with limited strong earthquake data. Earthq Spectra 2024;40(4):2692–711.
[20] Boore DM, Joyner WB. Site amplifications for generic rock sites. Bull Seismol Soc Am 1997;87(2):327–41.
[21] Atkinson GM, Boore DM. Earthquake ground-motion prediction equations for eastern North America. Bull Seismol Soc Am 2006;96(6):2181–205.
[22] Ohsaki Y. Dizhen dong de pu fenxi rumen [k] (Chinese Trans. Seismological Press; 2008. p. 134–5 (Original work published in Japanese).
[23] Boore DM. Smsim - Fortran programs for simulating ground motions from earthquakes: version 2.3 – a revision of OFR 96-80-A. Reston, VA: United States Geological Survey; 2005. Technical report.
[24] Boore DM. Stochastic simulation of high-frequency ground motions based on seismological models of the radiated spectra. Bull Seismol Soc Am 1983;73(6A):1865–94.
[25] Okada Y, Kasahara K, Hori S, Obara K, Sekiguchi S, Fujiwara H, Yamamoto A. Recent progress of seismic observation networks in Japan—Hi-net, F-net, K-NET and KiK-net—, 56. Earthquake, Planets and Space; 2004. xv-xxviii.
[26] Aoi S, Kunugi T, Nakamura H, Fujiwara H. Deployment of new strong motion seismographs of K-NET and KiK-net. Earthquake data in engineering seismology: predictive models. Data Manag Networks 2011:167–86.
[27] Zhang HZ, Zhao YG, Ge FW, Fang YC, Ochiai T. Estimation of input energy spectrum from pseudo-velocity response spectrum incorporating the influences of magnitude, distance, and site conditions. Eng Struct 2023;274:115165.
[28] Morikawa N, Iwaki A, Fujiwara H, Akiyama S, Maeda T, Kubo H, Aoi S, Hayakawa T, Takahashi M, Kato K, Tomozawa Y, Suzuki F, Motoki K, Iida T, Sato T, Ishii T, Miyakoshi J, Shimazu N, Oana A, Hayashi T, Kishida N, Okazaki T, Si H, Matsuyama H, Midorikawa S. Flat file of K-NET and KiK-net strong-motion records. In: Proceedings in the 18th world conference on earthquake engineering; 2024.
[29] Uchide T, Imanishi K. Underestimation of microearthquake size by the magnitude scale of the Japan meteorological agency: influence on earthquake statistics. J Geophys Res Solid Earth 2018;123(1):606–20.
[30] Council BSS. Recommended provisions for seismic regulations for new buildings and other structures. In: NEHRP (national earthquake Hazards Reduction Program); 2000. Washington, DC.
[31] Chiu HC. Stable baseline correction of digital strong-motion data. Bull Seismol Soc Am 1997;87(4):932–44.
[32] Sigurdsson SU, Rupakhety R, Sigbjörnsson R. Adjustments for baseline shifts in far-fault strong-motion data: an alternative scheme to high-pass filtering. Soil Dynam Earthq Eng 2011;31(12):1703–10.